Morphological transition behavior of *ABC* star copolymers by varying the interaction parameters

Ching-I Huang,* Hsin-Kai Fang, and Chih-Hao Lin
Institute of Polymer Science and Engineering, National Taiwan University, Taipei 106, Taiwan
(Received 5 October 2007; revised manuscript received 17 January 2008; published 20 March 2008)

We employ dissipative particle dynamics (DPD) to examine the effects of composition and interaction parameter on the resulting phase behavior of *ABC* star copolymers. Here, we assume that the interaction parameters among the three components are equal. When the three components have comparable volume fractions, our DPD results illustrate that the unique formation of various types of three-phase separated polygonal cylinders is mainly dominated by the composition but not influenced by the interaction parameter. In contrast, when two of the three components are minor, the resulting morphology type is greatly influenced by the interaction parameter. Generally speaking, with an increase in the interaction parameter, the two minority components first act like one component and the system forms a one-length-scale ordered microstructure. Then a further segregation between the two minority components within the large-length-scale phase can be induced as the interaction parameter keeps increasing. In general, our DPD results, a systematic study of the morphological transition behavior obtained by varying the interaction parameter and composition, bridge the gap between the previous theoretical results in the strong and weak segregation regimes via Monte Carlo and two-dimensional self-consistent mean-field methods, respectively.

DOI: 10.1103/PhysRevE.77.031804 PACS number(s): 61.41.+e, 64.70.Nd

I. INTRODUCTION

During the last three decades, *ABC* triblock copolymers have attracted wide attention due to their fascinating self-assembling behavior. Earlier studies have mainly focused on linear *ABC* triblock copolymers [1–5]. It was only in the last ten years that, with the improvement in synthetic techniques, morphological research on star-shaped *ABC* copolymers began to emerge from both experimental [6–19] and theoretical [20–25] points of view. Because of the topological constraint generated from the fact that three different polymer chains are connected at one junction point, *ABC* star copolymers display various geometric structures that cannot be formed in copolymers with linear architectures.

One of the unique phase-separated structures formed by *ABC* star copolymers is a cylindrical phase with polygonal cross sections, which is often denoted as a set of integers $[k.l.m....]$. To clarify, $[k.l.m....]$ represents that a k-gon, an l-gon, and an m-gon, etc. meet consecutively on each vertex in the cylindrical patterns. Figure 1 illustrates the four typical types of polygonal structures of [6.6.6], [8.8.4], [10.8.4;10.6.4], and [12.6.4], which have been discovered in the *ABC* star copolymers. Note that in the tiling pattern of [10.8.4;10.6.4] the longest block forms decagons, the second longer block has two types of octagons and hexagons, and the shortest block forms tetragons. By applying the imaginary tiling scheme as shown in Fig. 1, it has also been denoted as [3.3.4.3.4]. For instance, Matsushita and co-workers [13,16] synthesized a series of polyisoprene (PI)–polystyrene (PS)–poly(2-vinylpyridine) (P2VP) star copolymers with the composition ratio of PI:PS:P2VP equal to $1:1:X$. The resulting morphology patterns obtained via transmission electron microscopy and small-angle x-ray scattering display characteristic cylindrical structures of [6.6.6], [8.8.4], [10.8.4;10.6.4], and [12.6.4] with increasing P2VP composition X, which remains in the range of $0.7 \leq X \leq 1.9$. Furthermore, they observed the formation of cylinders in lamellae, lamellae within cylinders, and lamellae within spheres, in PI-PS-P2VP star copolymers with PI:PS:P2VP=$1:1.8:X$ in the range of $4.3 \leq X \leq 53$ [18].

Indeed, the phase behavior of *ABC* star copolymers is very diverse and complicated as it involves many important parameters, such as each block length and the immiscibility parameter between each pair of components I and J. Although some experimental work has successfully displayed various types of unique structures for *ABC* star copolymers, a thorough understanding of the morphological behavior resulting from varying these factors is hard to reach simply via experiments as it demands a lot of synthesis work. Accord-

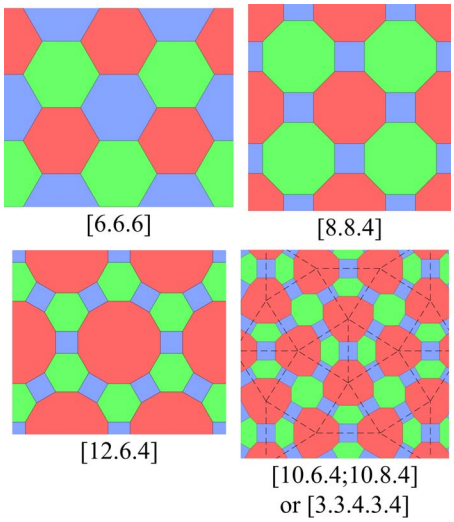

FIG. 1. (Color online) Schematic plot of the four types of polygonal structures frequently observed in *ABC* star copolymers.

*Author to whom correspondence should be addressed. FAX: 886-2-33665237. chingih@ntu.edu.tw

ingly, there have been a few related theoretical studies [20–25]. For example, Gemma *et al.* [21] adopted Monte Carlo (MC) simulations to examine the morphological behavior of *ABC* star copolymers with the composition ratio of $1:1:X$. They assumed that the three interaction parameters among these components are equal and in the strong segregation regime. By varying the composition X, various types of structures, lamellae+spheres, [8.8.4], [6.6.6], [8.6.4;8.6.6], [10.6.4;10.6.6], [12.6.4], perforated layers, lamellae+cylinders, columnar piled disks, and lamellae within spheres, have been predicted. Recently, the polygonal structure of [10.8.4;10.6.4] (i.e., [3.3.4.3.4]) has also been simulated in the *ABC* star copolymer with chain length ratios of 9:7:14 and 9:7:16 by the MC method [25]. Tang *et al.* [24] constructed the phase diagram for *ABC* star copolymers on the basis of a two-dimensional (2D) real space implementation of the self-consistent mean-field (SCMF) theory. When the three interaction parameters are equal, as in the work of Gemma *et al.* [21] but in the intermediate segregation regime, they obtained the same morphology patterns of polygonal cylinders, such as [8.8.4] and [6.6.6], and lamellae +cylinders, for comparable compositions of the three components; whereas when the composition of one of the three components is significantly larger and/or smaller than the other two components, the SCMF and MC approaches display different morphological behavior. For example, when $f_A=f_B \ll f_C$, the SCMF theory predicts the formation of hexagonally packed cylinders formed by the two miscible minority components A and B, which is different from the columnar piled disks (i.e., A and B segregated lamellae within cylinders) obtained by MC simulations. When $f_A=f_B \gg f_C$, though both SCMF and MC approaches predict a lamellar phase, the minority component C is shown to form a very thin layer and spheres, respectively, in the interfaces. These discrepancies indicate that, in addition to the dimensional difference of the simulation space, the interaction parameters (i.e., the segregation degree) play a very important role in the resulting morphological behavior of *ABC* star copolymers. This, however, has not been fully explored yet. Indeed, the occurrence of a systematic phase transition on varying the interaction parameters from weak to intermediate to even strong segregation is of great interest, and may be qualitatively observed experimentally by temperature variation.

In this paper, we thus employ the dissipative particle dynamics (DPD) simulation technique [26,27] to examine the self-assembling behavior of *ABC* star copolymers. Generally speaking, the DPD method simplifies a long series of molecular groups into a few bead-and-spring type particles, and therefore it can simulate the molecular behavior on longer time scales and larger length scales than the classical molecular dynamics and Monte Carlo simulations. Groot and Madden [28] were the first to successfully apply DPD to the microphase separation behavior of linear *AB* diblock copolymers. The phase diagram they constructed, though based on the results for short *AB* chains with the total number of beads per chain, N, equal to 10, is found in near quantitative agreement with that predicted by the SCMF theory [29], provided that the fluctuation effects caused by finite chains are included [30]. Similarly, we have employed DPD to examine the phase separation behavior for AB_2 three-arm star copolymers [31]. Our simulated phase diagram for AB_2 molecules with the total number of beads per chain, N, equal to 20 also captured most of the important morphological transitions occurring on varying the composition and interaction parameters, as predicted by SCMF theory [32]. Therefore, in this study we choose the total number of beads for an *ABC* three-arm molecule, as displayed in Fig. 2, to be fixed at $N=N_A+N_B+N_C=20$. These three arms are assumed to connect at one core bead (denoted as Y). In order to exclude the effects associated with the existence of the core bead, we set the Flory-Huggins interaction parameter between the core and each component of A, B, and C, equal to 0. Here, we aim to explore how the resulting morphology formation at various composition ratios of $f_A/f_B/f_C$ is influenced by the interaction parameters (a_{AB}, a_{AC}, and a_{BC}). For a comparison with current theoretical studies via the MC and SCMF approaches, we also set symmetric interaction parameters, i.e., $a_{AB}=a_{AC}=a_{BC}=a$, at the current stage. We will show that, even in this simplified case of $a_{AB}=a_{AC}=a_{BC}=a$, the *ABC* star copolymers, in particular when the composition of one of the three components is significantly large, display a series of quite interesting morphology transitions from a one-length-scale microstructure into a two-length-scale hierarchical structure within a structure as the interaction parameter changes. In general, the morphological transition behavior we display here, resulting from a systematic study with varying interaction parameter and composition, may provide insights into the structures associated with *ABC* copolymers.

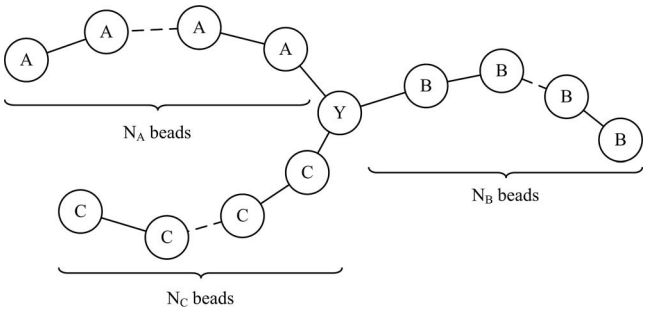

FIG. 2. Schematic plot of model *ABC* star copolymers.

II. DPD SIMULATION METHOD AND MODEL PARAMETERS

The DPD simulation method was originally proposed by Hoogerbrugge and Koelman [26] and first applied successfully by Groot and Madden [28] to the microstructures in linear *AB* diblock copolymer melts. The detailed formula can be found in Refs. [27] and [28], and will not be reiterated here. We previously have employed DPD to examine the phase separation behavior for amphiphilic molecules with various types of molecular architecture and/or in the presence of solvents [31,33–36]; the details of DPD are also given in those references.

In simulating the phase behavior of *ABC* star copolymers by DPD, the particle mass m, the cutoff radius r_c, and the temperature k_BT are all set equal to 1, for convenience. The

parameters γ and σ, which occur in the dissipative force and random force, respectively, are set to 4.5 and 3.0, respectively [27]. The connecting pairs of beads in a molecule are assumed to interact via a linear spring with a harmonic spring constant C equal to 4 [27]. The DPD simulations are performed in a cubic box of L^3 grids with periodic boundary conditions. The particle density ρ is set equal to 3. Hence, the total number of simulated DPD beads is $3L^3$. Initially these particles are started with a disordered configuration. Then the time evolution of the positions and velocities of all beads is carried out according to the velocity Verlet algorithm with $\lambda=0.65$ and the time step equal to 0.05 [37]. Each simulation is performed until the formed structure remains somewhat unchanged with further time steps.

The dimensionless interaction parameter (i.e., in terms of k_BT) between like particles a_{II} when the particle density $\rho=3$ is set equal to 25 according to the work of Groot and Warren [27]. The interaction parameter between different components I and J can be estimated by the following relationship between a_{IJ} and the Flory-Huggins interaction parameter χ_{IJ} derived by Groot and Warren [27] for $\rho=3$:

$$a_{IJ}(T) = a_{II} + 3.497\chi_{IJ}(T), \quad I,J = A,B,C. \tag{1}$$

Therefore, the value of $a_{IJ} \leq 25$ corresponds to $\chi_{IJ} \leq 0$, which indicates that components I and J are very miscible. As the immiscibility between I and J increases, a_{IJ} increases from 25. To ignore the effects of the junction point (Y), we assume that the Flory-Huggins interaction parameter between the core and each component is equal to 0 ($\chi_{IY}=0$), indicating that $a_{IY}=25$, $I=A,B,C$. In order to examine how the degree of incompatibility among these three components affects the self-assembling behavior of *ABC* star molecules, we set $a_{AB}=a_{AC}=a_{BC}=a>25$. It should be mentioned that the value of the Flory-Huggins interaction parameter χ_{IJ}, transformed directly from the interaction parameter in the DPD simulations, a_{IJ}, by Eq. (1) would not correspond to the true value of χ_{IJ} used in the SCMF theory. This is mainly due to the fact that in the DPD simulations our simulated copolymer chains are indeed very short ($N=20$) and thereafter the fluctuation effects become significant enough to stabilize the disordered regime; while the phase behavior predicted by the SCMF theory is appropriate for infinite chains ($N\rightarrow\infty$). To clarify, a further mapping of χN for a finite chain length onto $(\chi N)_{\text{eff}}$ for an infinite chain length has to be achieved in order to quantitatively compare the phase behaviors determined from DPD and SCMF theory. As far as we know, this conversion has not been derived theoretically for *ABC* miktoarm star copolymers. Hence, in this study we systematically examine the self-assembling behavior by gradually increasing the value of the interaction parameter; the results can be compared with those predicted by the SCMF and MC approaches on increasing the value of χN only qualitatively.

In general, the resulting morphology patterns obtained via DPD are dependent on the finite size of the simulation box, as reported in other theoretical studies [20,38,39]. In order to exclude the finite-size effects, one has to keep enlarging the simulation box size until the structures are no longer affected by the simulation box. For example, Fig. 3(a) illustrates the structure patterns for *ABC* star molecules with

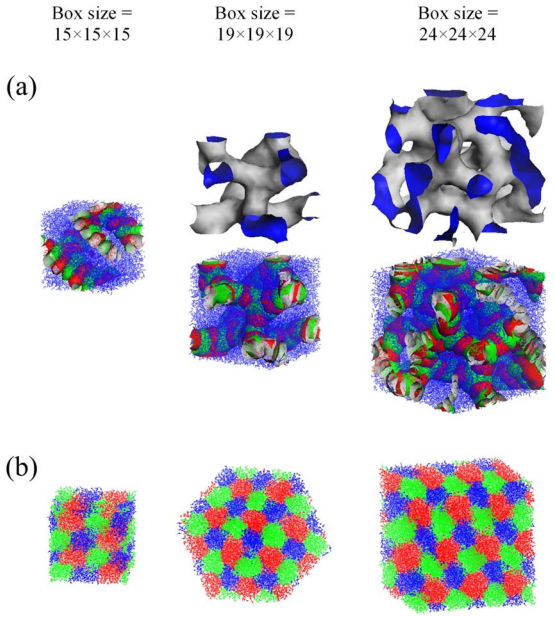

FIG. 3. (Color online) Morphology patterns of *ABC* star copolymers for (a) $f_A/f_B/f_C=0.1/0.1/0.8$ at $a=70$ and (b) $f_A/f_B/f_C=0.35/0.35/0.3$ at $a=36$, simulated in different box sizes. The red, green, and blue colors represent A, B, and C, respectively. The red, green, and blue surfaces correspond to the isosurfaces of components A, B, and C, respectively.

composition $f_A/f_B/f_C=0.1/0.1/0.8$ at the interaction parameter $a=70$, simulated in different box sizes. It is clear that, when the simulation box size is $15\times15\times15$, the two minority components A and B form segregated oblate spherical or disklike micelles within the AB-formed perforated layers; whereas when the box size is expanded to $19\times19\times19$ and $24\times24\times24$, these micelles alternately packed of A and B form within the 3D network. These phases will be explained in detail later. In Fig. 3(b) we also display the corresponding structure patterns with respect to different box sizes for comparable values of the composition $f_A/f_B/f_C=0.35/0.35/0.30$ at $a=36$. For the simulation box between $15\times15\times15$ and $24\times24\times24$, we observe the same formation of [6.6.6]. These results indicate that, for our current model systems with the total number of beads per chain $N=20$, the simulation box size of $19\times19\times19$ is large enough to ensure that finite-size effects will not influence the morphological results. All the structure patterns analyzed below are obtained within the $19\times19\times19$ box. In each simulated morphology pattern, the red, green, and blue colors are used to represent A, B, and C, respectively.

III. RESULTS AND DISCUSSION

In order to highlight the effects of composition on the resulting morphological behavior, we choose the symmetric interaction parameter $a=36$ and construct the corresponding phase triangle in terms of three compositions f_A, f_B, and f_C in Fig. 4. Owing to the special molecular architecture of *ABC* star copolymers as well as the equal interaction parameters among these three blocks, switching the sequence of A, B,

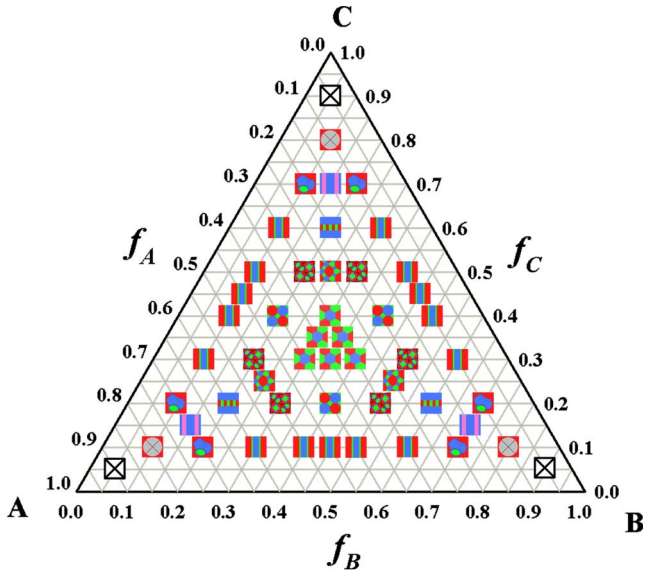

FIG. 4. (Color online) Phase triangle of *ABC* star copolymers simulated at $a=36$. In the figure, ( ) [6.6.6]; ( ) [8.8.4]; ( ) [10.6.4;10.8.4] (3.3.4.3.4); ( ) [10.6.6;10.6.4]; ( ) C_I+C_J within L (*I* and *J* are minority components); ( ) $L_{I,J}$ with *K* in the interfaces (*I* and *J* are majority components); ( ) *I*- and *J*-segregated domains within L (*I* and *J* are minority components); ( ) gyroid; ( ) *IJ*-formed tubes (*I* and *J* are minority components); ( ) disorder.

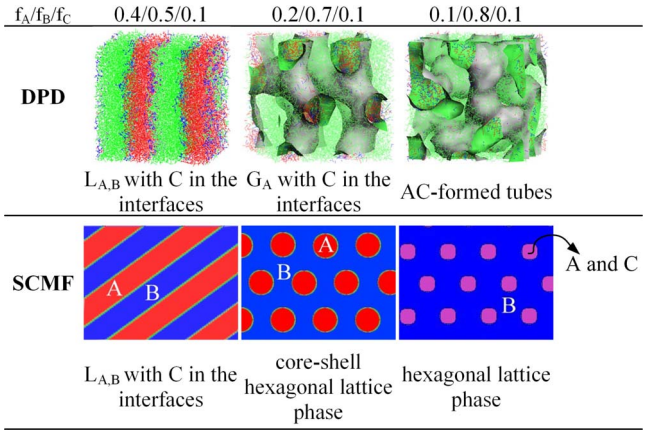

FIG. 5. (Color online) Morphology variation of *ABC* star copolymers with f_A at a fixed value of $f_C=0.1$ and $a=36$. The red, green, and blue colors represent *A*, *B*, and *C*, respectively. The green surface corresponds to the isosurface of component *B*. Here we include the simulated results via the SCMF method [24] as a comparison.

and *C* blocks does not change the phase symmetry, and therefore the phase triangle displays a permutation symmetry with respect to *A*-*B*, *B*-*C*, and *C*-*A*. In view of the phase diagram constructed when $a=36$, as shown in Fig. 4, most of the resulting simulated microstructures formed by the *ABC* star copolymers can be displayed along two lines of varying the compositions of f_A, f_B, and f_C.

First, when one of the three composition values f_C (or f_A or f_B) is comparatively small, the resulting phase behavior is similar to linear diblock copolymers. For example, Fig. 5 presents a series of microstructure transition with f_A when f_C is fixed at 0.1. Here, we also include the characteristic 2D morphology patterns obtained by the SCMF theory as a comparison [24]. When $0.3 \leq f_A \leq 0.45$ (i.e., $0.6 \geq f_B \geq 0.45$), since the *A* and *B* compositions are comparable, the systems segregate to form *A*-rich and *B*-rich lamellae ($L_{A,B}$) with the minority component *C* in the interfaces. This structure was also observed by the SCMF theory. As the composition f_A decreases to 0.2 ($f_B=0.7$), the formed microstructure turns into a gyroid of *A* (G_A) with the minority *C* still in the interfaces. When f_A decreases further to 0.1 ($f_B=0.8$), since both *A* and *C* are minor components, the interaction parameter $a=36$ is not significant enough to assure the segregation between *A* and *C*. Therefore, these two minor components are favored to mix together to form tubes in the majority *B* matrix (*AC*-formed tubes). Recall that, when $f_C=0.1$, the SCMF theory shows a transition from $L_{A,B}$ with *C* in the interfaces $\rightarrow$ hexagonally packed *A*-formed cylinders (C_A^{hex}) with *C* in the interfaces $\rightarrow$ hexagonally packed *AC*-formed cylinders (C_{AC}^{hex}) with decreasing f_A. Both approaches predict the same distribution trend of each component. However, the resulting morphology types for the two systems with $f_A/f_B/f_C=0.2/0.7/0.1$ and 0.1/0.8/0.1 are different. This may be attributed to the dimensional difference of the simulation space and/or the interaction parameters. Later we will show that, by varying the interaction parameters, the *ABC* star copolymers, in particular when two of the three components are minor, can display a variety of more complex 3D hierarchical structures, which cannot be observed by the 2D SCMF simulations.

Next, in Fig. 6 we present the simulated morphology patterns via DPD at various values of f_C along the symmetric composition line of *A* and *B*, i.e., $f_A=f_B=(1-f_C)/2$. When $f_C=0.1$, the structure formed is $L_{A,B}$ with *C* in the interfaces, as stated before. As the *C* composition increases to ≥ 0.2, since the amount of *C* is sufficient to self-assemble and destroy the previously formed *A* and *B* segregated lamellae, three-phase separated microstructures are formed. As predicted in other theoretical studies [21,24], various types of polygonal cylinders, [8.8.4], [6.6.6], and [10.6.6; 10.6.4], have also been observed via DPD when f_C is equal to 0.2, 0.3–0.4, and 0.5, respectively. As expected, the number of vertices of polygons displays a roughly proportional relationship with the composition. With the increase of the *C* composition f_C from 0.2 to 0.5, the *C*-formed polygons transform from tetragons $\rightarrow$ hexagons $\rightarrow$ decagons; while the cylindrical domains formed by *A* or *B* blocks vary from octagons $\rightarrow$ hexagons $\rightarrow$ coexistence of hexagons and tetragons. It should be mentioned that, when $f_C=0.5$, though we observe the formation of a coexistence of cylindrical structures [10.6.6] and [10.6.4] in the simulation box of $19\times19\times19$, it is hard to identify the formed morphology types in larger simulation boxes. This is reasonable mainly because the region $f_C \cong 0.5$ is marginal between the cylindrical and lamellar phases. Indeed, our observation via DPD for the system with $f_C=0.5$ is in concord with the MC conclusion that no single unique microstructure forms at this composition value

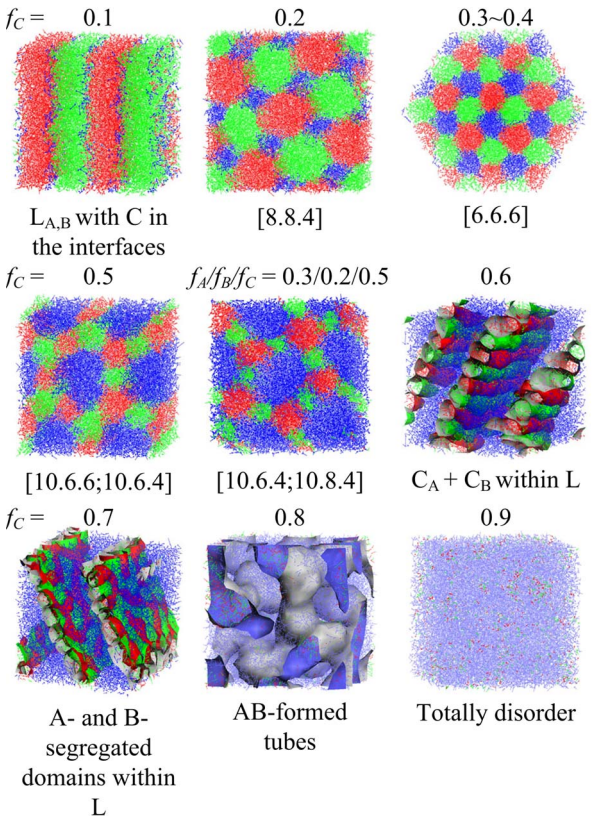

FIG. 6. (Color online) Morphology variation of *ABC* star copolymers with f_C when $f_A=f_B=(1-f_C)/2$ and $a=36$. The red, green, and blue colors represent *A*, *B*, and *C*, respectively. The red, green, and blue surfaces correspond to the isosurfaces of components *A*, *B*, and *C*, respectively.

[21]. Instead, three possible phases appeared in different simulation boxes via the MC method. Two of them are cylindrical structures of [10.6.6;10.6.4] and [12.6.4]. In the other one the majority *C* blocks form perforated layers (PL_C), while the minority *A* and *B* segregate to form alternately arranged cylinders in *AB*-rich layers and penetrate into the holes of the *C* layers (denoted as C_A+C_B within PL_C). In addition to these types of polygonal cylinders, we observe another kind of cylindrical phase via DPD, [10.6.4;10.8.4] (i.e., [3.3.4.3.4]), which typically forms at $f_A/f_B/f_C=0.3/0.2/0.5$ or 0.2/0.3/0.5. It should be noted that when the three interaction parameters are equal, we observe this phase easily when $f_A=f_B$ and f_C is around 0.5 instead of the structure [12.6.4] most frequently observed via MC simulation, though [3.3.4.3.4] has also been simulated via the MC method with the chain length ratios of 9:7:14 and 9:7:16 [25]. However, when the three interaction parameters are no longer symmetric, it is easy to observe the formation of [12.6.4] via DPD. For example, when we vary the three interaction parameters from the equal case to $a_{BC}>a_{AB}=a_{AC}$, i.e., the interaction between *B* and *C* is significantly larger than that between *A* and *B* (*C*), the *ABC* star copolymer with $f_A/f_B/f_C=0.25/0.25/0.5$ can transform easily from [10.6.6;10.6.4] into [12.6.4]. This is not surprising because the *B* and *C* blocks tend to avoid contact with each other and thus stretch more into their respective domains. This behavior is analogous to increasing the volume fractions of *B* and *C*. Accordingly, the vertex number of polygons formed by the majority *C* and minority *B* increases from 10 to 12, and the coexistence of 6 and 4 to 6, respectively; whereas the minority *A*-formed polygons transform from coexistence of hexagons and tetragons to only tetragons. In fact, Takano *et al.* [13] found the same [12.6.4] structure in the PS-PI-P2VP star copolymer with composition ratio around 025:0.25:0.5. A systematic investigation varying the symmetry of the interaction parameters will be given in the future.

Now we continue to discuss the systems with f_C increasing to ≥ 0.6, in which both compositions f_A and f_B are smaller than f_C and hence the three-phase separated polygonal cylinders are no longer formed. For example, when $f_A=f_B=0.2$ and $f_C=0.6$, the morphology pattern in Fig. 6 shows a *C*-rich and an *AB*-rich lamellar phase with *A*- and *B*-formed cylinders alternately packed in the *AB*-rich layers (C_A+C_B within L). As f_C increases further to 0.7, though a lamellar phase is still formed, the amounts of *A* and *B* are not enough to form well-ordered cylinders. Therefore we observe the formation of *A*- and *B*-segregated domains within the *AB*-rich lamellae when $f_C=0.7$. Furthermore, when f_C becomes even larger, these two minority components *A* and *B* can no longer separate from each other at lower values of the interaction parameters. Accordingly, we observe a tube-like and a disordered phase at $f_C=0.8$ and 0.9, respectively.

Compared to the morphological results for the systems with $f_A=f_B=(1-f_C)/2$ by the MC and SCMF methods, which correspond to the strong and weak segregations regimes, respectively, we see that, when f_C lies in the range of $0.2\leq f_C\leq 0.5$, the three approaches predict structures with even-numbered polygonal cylinders. In contrast, when $f_C\geq 0.6$, the resulting morphology patterns simulated by these three approaches are different, indicating that the formation of ordered structures for *ABC* star copolymers in this composition range is strongly influenced by the interaction parameters. In addition, it has been clearly shown by both DPD and MC methods that more complex 3D structure-within-structures are formed quite often for systems where $f_C\geq 0.6$. Accordingly, one may not obtain the structure information correctly for this regime by the SCMF method in 2D.

To illustrate the effects of the interaction parameter *a* on the structure formation, we systematically vary the symmetric interaction parameter *a* and examine the morphology patterns for a series of systems along the symmetric composition line of $f_A=f_B=(1-f_C)/2$. Figure 7 presents the corresponding phase diagram in terms of f_C and *a*. Based on how the morphological behavior is affected by the interaction parameter, the *ABC* star copolymers can be divided into two main regimes. First, for systems with $f_C\leq 0.5$, provided that the interaction parameter *a* is large enough to exceed the order-disorder transition value, the formed morphology is almost uninfluenced by the interaction parameter and mainly dominated by the composition. A series of transitions from $L_{A,B}$ with *C* in the interfaces, ($f_C=0.1$)$\rightarrow$[8.8.4], ($f_C=0.2$)$\rightarrow$[6.6.6], ($f_C=0.3-0.4$)$\rightarrow$[10.6.6;10.6.4], ($f_C=0.5$), is observed, which has been clearly manifested previously and will not be reiterated here. Our DPD results in this composition regime confirm that the simulated morphology patterns in the strong and weak segregation regimes via MC and

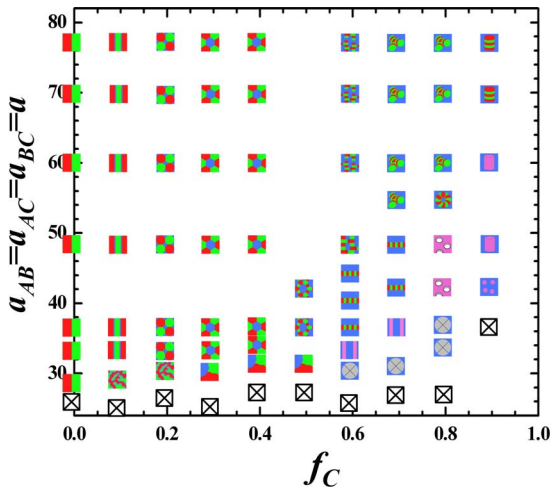

FIG. 7. (Color online) Phase diagram of *ABC* star copolymers with symmetric compositions of *A* and *B* ($f_A=f_B$) in terms of the interaction parameter a and composition f_C. In the figure, ( ) $L_{A,B}$; ( ) $L_{A,B}$ with *C* in the interfaces; ( ) [8.8.4]; ( ) [6.6.6]; ( ) [10.6.6;10.6.4]; ( ) C_A+C_B within L; ( ) C_A+C_B within PL_C; ( ) C_A+C_B within PL_{AB} and PL_C; ( ) $SWM_{A,B}$ within 3D network; ( ) $SWM_{A,B}$ within PL_{AB}; ( ) $SWM_{A,B}$ within C_{AB}^{hex}; ( ) *A*- and *B*-segregated domains; ( ) *A*-, *B*-, and *C*-segregated domains; ( ) *A*- and *B*-segregated domains within L; ( ) *A*- and *B*-segregated domains within PL_{AB}; ( ) *AB*-formed micelles; ( ) $C_{A/B}^{hex}$; ( ) *AB*-formed tubes; ( ) disorder.

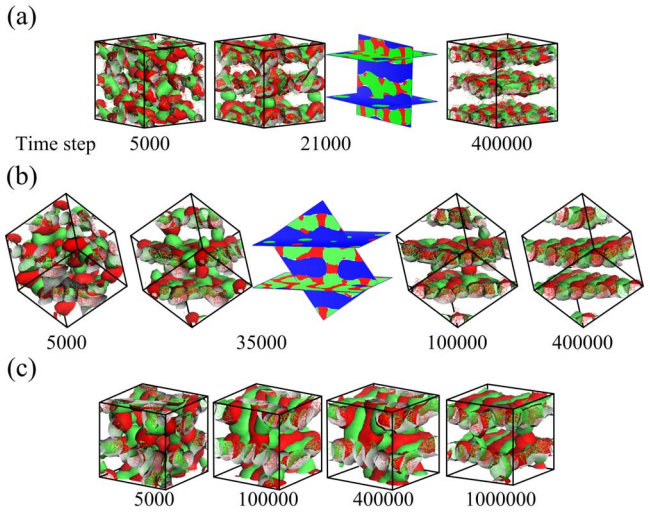

FIG. 8. (Color online) Time-resolved morphology patterns of *ABC* star copolymers with symmetric compositions of *A* and *B* ($f_A=f_B$) when $f_C=0.6$ and the interaction parameter $a=$ (a) 33, (b) 44, and (c) 48, respectively. The red and green colors represent *A* and *B*, respectively. The red, green, and blue surfaces correspond to the isosurfaces of components *A*, *B*, and *C*, respectively. For clarity, we omitted the *C* blocks in the patterns.

SCMF methods are identical. As the interaction parameter a decreases, the ordered *ABC* star copolymers are expected to become disordered. However, due to the effects of thermal fluctuations, we observe that, between the totally disordered and the well-ordered states, the systems tend to form a micellelike structure, i.e., with chains aggregating as large droplets but no formation of well-ordered structures. As expected, we observe a micellelike structure of *A*- and *B*-segregated domains when two of the three components *A* and *B* are major components, such as for $f_C \leq 0.2$, and *A*-, *B*-, and *C*-segregated domains for systems when the three components are comparable, such as for $f_C=0.3-0.5$.

When $f_C \geq 0.6$, so that two of the components *A* and *B* are significantly minor, we find that a series of morphology transitions can be induced by varying the interaction parameter a. As expected, with increasing interaction parameter a, the two minority components *A* and *B* first act like one component, and the system separates into *AB*-rich and *C*-rich phases; then a further segregation between the two minority components *A* and *B* occurs within the *AB*-rich phases and the system forms the so-called hierarchical structures within structures. For example, when $f_C=0.6$, the disordered system first transforms into *AB*-formed tubes and then undergoes a series of four types of well-ordered morphology transitions of *A*- and *B*-segregated domains within $L \rightarrow C_A+C_B$ within $L \rightarrow C_A+C_B$ within $PL_C \rightarrow C_A+C_B$ within PL_{AB} and PL_C as the interaction parameter a keeps increasing. In Figs. 8(a)–8(c) we present the time evolution of these structures which are simulated for $f_C=0.6$ at $a=33$, 44, and 48, respectively. As can be seen clearly in Fig. 8(a), when the interaction parameter a is lower ($a=33$), the system decomposes very quickly to form an *AB*-rich 3D interconnected network in the presence of the majority *C* component, within which one can observe segregation between the two minority components *A* and *B*. As the time step increases, this interconnected microstructure gradually turns into a lamellar structure; further, it is interesting to observe that the *A*- and *B*-segregated domains still remain the same without getting coarsened within the *AB*-rich layers. This is not surprising because of the lower values of the interaction parameter a. If we further increase the interaction parameter a, one may expect that these *A*- and *B*-segregated domains become coarsened in order to reduce the surface free energy and hence form *A* and *B* cylinders alternately arranged within the *AB*-rich layers (C_A+C_B within L), as displayed in Fig. 8(b) when $a=44$. In addition, the time-evolved patterns clearly show a series of large-length-scale morphology transitions from a 3D interconnected structure $\rightarrow PL_{AB}$ and PL_C (i.e., the *AB*-rich and *C*-rich layers are perforated by *C* and *A* or *B* domains, respectively) $\rightarrow PL_C \rightarrow L$. As the interaction parameter becomes larger, for example $a=48$, as shown in Fig. 8(c), because the two minority *A* and *B* components would like to segregate to reduce their interfacial area, both *A* and *B* have a tendency to form oblate spheres in the very early separation stages. Accordingly, we observe a slower coarsening process of these *A* and *B* spherical-like domains into cylinders as well as the large-length-scale ordering transformation. Though the systems undergo a similar morphology evolution with time as in the case of $a=44$, the simulated structure pattern at $a=48$ up to 10^6 time steps shows the formation of C_A+C_B within PL_C. As the interaction parameter a becomes even larger (≥ 60) so that the coarsening process is further slowed, we observe the formation of C_A+C_B within PL_{AB} and PL_C when the time step reaches 10^6. The fact that increasing the interaction parameter a

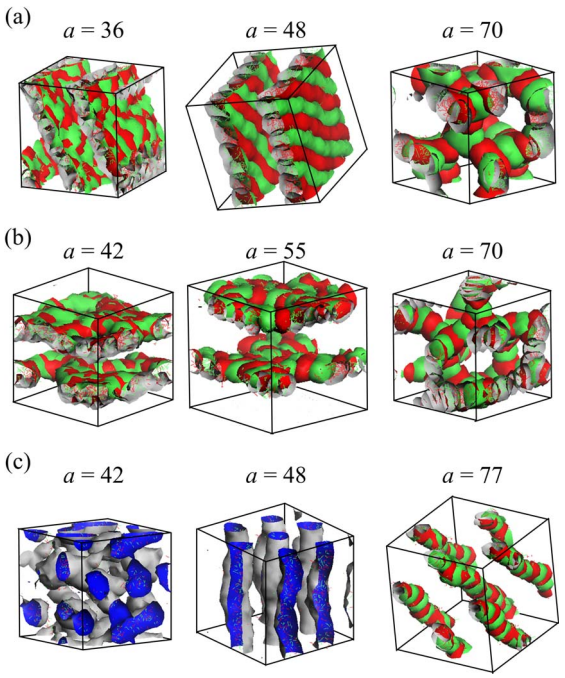

FIG. 9. (Color online) Morphology variation of *ABC* star copolymers with the interaction parameter a for systems with symmetric compositions of A and B ($f_A=f_B$) when $f_C=$ (a) 0.7, (b) 0.8, and (c) 0.9, respectively. The red and green colors represent A and B, respectively. The red, green, and blue surfaces correspond to the isosurfaces of components A, B, and C, respectively. For clarity, we omitted the C blocks in the patterns.

enables the A and B minority components to form alternately packed spherical or disklike domains instead of cylindrical domains can be seen more obviously when f_C increases to 0.7 in Fig. 9(a). When the interaction parameter $a<50$, two types of morphologies, A- and B-segregated domains within L ($a=36$) and C_A+C_B within L ($40<a<50$), are formed, as in the system of $f_C=0.7$. As a continues to increase further, we observe the formation of segmented A and B wormlike micelles ($SWM_{A,B}$) within a 3D network. To clarify, the A and B minority components respectively form oblate spherical micelles, which alternately pack to form a 3D wormlike network. Indeed, the alternately segmented A and B micelles can be formed in a wide range of $f_C\geq 0.7$. Figures 9(b) and 9(c) illustrate the characteristic morphology patterns as a function of the interaction parameter a formed by the systems with $f_C=0.8$ and 0.9, respectively. When $f_C=0.8$, we first observe the formation of A- and B-segregated domains within PL_{AB} in the range of $40<a<50$, and then these minority A and B domains can form alternately arranged wormlike micelles within PL_{AB} or the 3D network as the interaction parameter a keeps increasing. As increases to 0.9, since the compositions of A and B are very minor, the ordered structures formed are no longer lamellae or perforated layers. Instead, we observe hexagonally packed AB-formed cylinders (C_{AB}^{hex}), within which the two minority components A and B are first miscible together and then segregate to form alternately piled disklike micelles, as the interaction parameter a increases.

As manifested above, in addition to the three-phase separated polygonal structures, we successfully obtain other types of hierarchical structures, such as C_A+C_B within L, $SWM_{A,B}$ within PL or a 3D network, and $SWM_{A,B}$ within C_{AB}^{hex}, in the *ABC* star copolymer systems with $f_A=f_B=(1-f_C)/2$ and symmetric interaction parameters, i.e., $a_{AB}=a_{AC}=a_{BC}=a$. Typically, the systems form C_A+C_B within L when $f_C=0.6-0.7$, and gradually transform into $SWM_{A,B}$ within the 3D network and then $SWM_{A,B}$ within C_{AB}^{hex} on decreasing the compositions of A and B (i.e., increasing f_C) and/or increasing the interaction parameter a. In general, our DPD results, as a systematic study of the morphological transition behavior obtained by varying the interaction parameter and composition, bridge the gap between the previous theoretical results in strong and weak segregation regimes obtained via MC and 2D SCMF methods, respectively. Recall that Matsushita and co-workers have also observed a similar transition from C_A+C_B within L (which they called cylinders in lamellae) to $SWM_{A,B}$ within C_{AB}^{hex} (lamellae within cylinders) in PI-PS-P2VP star copolymers on varying the composition ratio [18]. However, they did not observe the formation of $SWM_{A,B}$ within the PL or 3D network, as predicted in our DPD simulations. We infer that this may be due to the fact that we set equal interaction parameters among the three components in our simulations; whereas PI-PS-P2VP copolymers have the relationship of the Flory-Huggins interaction parameters $\chi_{PI\text{-}P2VP}\gg\chi_{PI\text{-}PS}\approx\chi_{PS\text{-}P2VP}$. A further study of how the resulting phase behavior is affected by the asymmetry of the interaction parameters among these three components will be presented in the future. Indeed, the presence of a complex phase such as PL has been frequently located between the lamellar and cylindrical phases in copolymers. Recently, the so-called segmented wormlike hierarchical structure has been observed experimentally in *ABC* star copolymer solutions [40–42].

IV. CONCLUSIONS

We employed dissipative particle dynamics to examine the morphological transition behavior of *ABC* star copolymers. In particular, we assume that the interaction parameters among these three components are the same, and focus on the effects of composition and interaction parameter. When one of the components is a relatively minor block, so that it cannot self-assemble to form one phase, the phase behavior is similar to that of linear diblock copolymers, as expected. When the compositions of the three blocks are comparable, three-phase separated polygonal cylinders, [8.8.4], [6.6.6], [10.6.6; 10.6.4], and [10.6.4;10.8.4] (i.e., [3.3.4.3.4]), are formed. Our DPD results manifest the fact that the formation of these polygonal phases is strongly dominated by the composition but not influenced by the interaction parameter. Accordingly, the simulated morphology patterns via DPD in this composition region are in excellent agreement with those via the 2D real space approach of the SCMF method in the weak segregation regime and MC simulation in the strong segregation regime. In contrast, when two of the three components become minor, it is interesting to find that, in addition to the composition, the interaction parameter also

plays an important role in the resulting morphology types. Generally speaking, with increasing interaction parameter, the two minority components first act like one component and the system forms a one-length-scale ordered microstructure, as in linear diblock copolymers. Then a further segregation between the two minority components occurs within the large-length-scale phase as the interaction parameter keeps increasing, and the system can form the so-called hierarchical structures within structures. In addition to the formation of alternately packed cylinders within lamellae, since increasing the interaction parameter and/or decreasing the compositions of the two minority blocks enables these two minority components to form alternately piled wormlike micelles (oblate spheres or disks), two other types of hierarchical morphologies, segmented wormlike micelles within 3D network and segmented wormlike micelles within cylinders, have also been widely observed via DPD.

ACKNOWLEDGMENTS

This work was supported by the National Science Council of the Republic of China through Grant No. NSC 96-2221-E-002-019.

[1] Y. Mogi, K. Mori, Y. Matsushita, and I. Noda, Macromolecules **25**, 5412 (1992).
[2] Y. Mogi, H. Kotsuji, Y. Kaneko, K. Mori, Y. Matsushita, and I. Noda, Macromolecules **25**, 5408 (1992).
[3] S. P. Gido, D. W. Schwark, E. L. Thomas, and M. Goncalves, Macromolecules **26**, 2636 (1993).
[4] W. Zheng and Z.-G. Wang, Macromolecules **28**, 7215 (1995).
[5] P. Tang, F. Qiu, H. D. Zhang, and Y. L. Yang, Phys. Rev. E **69**, 031803 (2004).
[6] N. Hadjichristidis, H. Iatrou, S. K. Behal, J. J. Chludzinski, M. M. Disko, R. T. Garner, K. S. Liang, D. J. Lohse, and S. T. Milner, Macromolecules **26**, 5812 (1993).
[7] S. Okamoto, H. Hasegawa, T. Hashimoto, T. Fujimoto, H. Zhang, T. Kazama, A. Takano, and Y. Isono, Polymer **38**, 5275 (1997).
[8] S. Sioula, N. Hadjichristidis, and E. L. Thomas, Macromolecules **31**, 5272 (1998); **31**, 8429 (1998).
[9] H. Huckstadt, A. Gopfert, and V. Abetz, Macromol. Chem. Phys. **201**, 296 (2000).
[10] H. Huckstadt, T. Goldacker, A. Gopfert, and V. Abetz, Macromolecules **33**, 3757 (2000).
[11] V. Abetz, in *Encyclopedia of Polymer Science and Technology*, edited by J. I. Kroschwitz (John Wiley & Sons, New York, 2003).
[12] K. Yamauchi, K. Takahashi, H. Hasegawa, H. Iatrou, N. Hadjichristidis, T. Kaneko, Y. Nishikawa, H. Jinnai, T. Matsui, H. Nishioka, M. Shimizu, and H. Furukawa, Macromolecules **36**, 6962 (2003).
[13] A. Takano, S. Wada, S. Sato, T. Araki, K. Hirahara, T. Kazama, S. Kawahara, Y. Isono, A. Ohno, N. Tanaka, and Y. Matsushita, Macromolecules **37**, 9941 (2004).
[14] K. Yamauchi, S. Akasaka, H. Hasegawa, H. Iatrou, and N. Hadjichristidis, Macromolecules **38**, 8022 (2005).
[15] A. Takano, W. Kawashima, A. Noro, Y. Isono, N. Tanaka, T. Dotera, and Y. Matsushita, J. Polym. Sci., Part B: Polym. Phys. **43**, 2427 (2005).
[16] K. Hayashida, W. Kawashima, A. Takano, Y. Shinohara, Y. Amemiya, Y. Nozue, and Y. Matsushita, Macromolecules **39**, 4869 (2006).
[17] K. Hayashida, A. Takano, S. Arai, Y. Shinohara, Y. Amemiya, and Y. Matsushita, Macromolecules **39**, 9402 (2006).
[18] K. Hayashida, N. Saito, S. Arai, A. Takano, N. Tanaka, and Y. Matsushita, Macromolecules **40**, 3695 (2007).
[19] K. Hayashida, T. Dotera, A. Takano, and Y. Matsushita, Phys. Rev. Lett. **98**, 195502 (2007).
[20] Y. Bohbot-Raviv and Z.-G. Wang, Phys. Rev. Lett. **85**, 3428 (2000).
[21] T. Gemma, A. Hatano, and T. Dotera, Macromolecules **35**, 3225 (2002).
[22] X. He, L. Huang, H. J. Liang, and C. Y. Pan, J. Chem. Phys. **118**, 9861 (2003).
[23] T. M. Birshtein, A. A. Polotsky, and V. Abetz, Macromol. Theory Simul. **13**, 512 (2004).
[24] P. Tang, F. Qiu, H. D. Zhang, and Y. L. Yang, J. Phys. Chem. B **108**, 8434 (2004).
[25] K. Ueda, T. Dotera, and T. Gemma, Phys. Rev. B **75**, 195122 (2007).
[26] P. J. Hoogerbrugge and J. M. V. A. Koelman, Europhys. Lett. **19**, 155 (1992).
[27] R. D. Groot and P. B. Warren, J. Chem. Phys. **107**, 4423 (1997).
[28] R. D. Groot and T. J. Madden, J. Chem. Phys. **108**, 8713 (1998).
[29] M. W. Matsen and F. S. Bates, Macromolecules **29**, 1091 (1996).
[30] G. H. Fredrickson and E. Helfand, J. Chem. Phys. **87**, 697 (1987).
[31] C. I. Huang and H. T. Yu, Polymer **48**, 4537 (2007).
[32] G. M. Grason and R. D. Kamien, Macromolecules **37**, 7371 (2004).
[33] C. I. Huang and C. M. Chen, ChemPhysChem **8**, 2588 (2007).
[34] C. I. Huang and Y. C. Lin, Macromol. Rapid Commun. **28**, 1634 (2007).
[35] C. I. Huang, Y. J. Chiou, and Y. K. Lan, Polymer **48**, 877 (2007).
[36] C. I. Huang, H. Y. Hsueh, Y. K. Lan, and Y. C. Lin, Macromol. Theory Simul. **16**, 77 (2007).
[37] M. P. Allen and D. J. Tildesley, *Computer Simulation of Liquids* (Clarendon, Oxford, 1987).
[38] U. Micka and K. Binder, Macromol. Theory Simul. **4**, 419 (1995).
[39] Q. Wang, P. F. Nealey, and J. J. de Pablo, Macromolecules **34**, 3458 (2001).
[40] Z. Li, E. Kesselman, Y. Talmon, M. A. Hillmyer, and T. P. Lodge, Science **306**, 98 (2004).
[41] Z. Li, M. A. Hillmyer, and T. P. Lodge, Nano Lett. **6**, 1245 (2006).
[42] Z. Li, M. A. Hillmyer, and T. P. Lodge, Langmuir **22**, 9409 (2006).